

## Partial Oxidation of Gasoline over Ni/Al<sub>2</sub>O<sub>3</sub> Catalysts using Nickel Aluminate as Precursor

Ruben López-Fonseca\*, Cristina Jiménez-González, Miryam Gil-Calvo, Beatriz de Rivas, Jose-Ignacio Gutiérrez-Ortiz

Department of Chemical Engineering, Faculty of Science and Technology, University of The Basque Country UPV/EHU, P.O. Box 644, E-48080 Bilbao, Spain  
[ruben.lopez@ehu.eus](mailto:ruben.lopez@ehu.eus)

Gasoline, which currently presents a well-developed distribution network, represents an ideal fuel source for H<sub>2</sub> production onboard or in stationary facilities. In this work, a novel alumina supported Ni (NiAl<sub>2</sub>O<sub>4</sub>/Al<sub>2</sub>O<sub>3</sub>) catalyst derived from the reduction of nickel aluminate at high temperature was investigated for the partial oxidation of isooctane, which was selected as a gasoline surrogate. While being relatively active in the process due to its small crystallite size, the catalyst did not show a stable behavior with time on stream since a considerably coke formation was noticed. Interestingly a better performance in terms of conversion, yield of hydrogen and stability was observed when water was added to the feedstream.

### 1. Introduction

Low-temperature fuel cells are considered viable candidates for direct electricity production from hydrogen for transportation applications and also for distributed and portable power generation. However, the absence of a feasible hydrogen storage option and a hydrogen marketing infrastructure, at least in the near term, necessitate the search for an appropriate fuel. In this sense, gasoline, which already presents a well-developed distribution network, represents an ideal fuel source for H<sub>2</sub> production onboard or in stationary facilities supplying refuelling stations with H<sub>2</sub>. Moreover, gasoline has both a higher energy density and larger hydrogen content when compared with oxygenated hydrocarbons such as methanol and ethanol (Moon et al., 2004). In this work, isooctane has been selected as a gasoline surrogate and its conversion to H<sub>2</sub> by partial oxidation has been explored for the following reasons: (i) the reaction, C<sub>8</sub>H<sub>18</sub> + 4O<sub>2</sub> → 8CO + 9H<sub>2</sub>, (ΔH<sub>R</sub>(25 °C) = - 627 kJ·mol<sup>-1</sup>), is exothermic, making it much more energy-efficient than steam reforming; (ii) a smaller reformer can be used to achieve a high conversion of the hydrocarbon selectively in favour of the production of H<sub>2</sub> at short contact times; and (iii) the partial oxidation setup is more compact and mechanically simpler than the steam reforming, since no additional heating is required.

On the other hand, nickel-based catalysts offer a good compromise between cost and reforming behaviour in spite of the fact that its operation is frequently accompanied by coking. Most studies related to this class of catalysts use nickel oxide as a precursor to obtain active metallic nickel after reduction. An alternative approach for synthesis is to stabilise nickel within a well-defined crystalline oxide nickel aluminate (NiAl<sub>2</sub>O<sub>4</sub>). The potential of this precursor for methane reforming by partial oxidation, steam reforming or dry reforming has been successfully reported (López-Fonseca et al., 2012). With the aim of optimising the mass catalytic activity of the nickel active phase it seems reasonable to incorporate the spinel on a high specific surface support. Alumina can be considered a suitable candidate given the structural and chemical compatibility with reduced NiAl<sub>2</sub>O<sub>4</sub>, which results in Ni/Al<sub>2</sub>O<sub>3</sub>. In this regard our recent results on this type of catalyst formulation prepared by precipitation pointed out that NiAl<sub>2</sub>O<sub>4</sub>/Al<sub>2</sub>O<sub>3</sub> catalysts (10-24 w/w % Ni loading) exhibited a comparable reforming activity than a bulk spinel sample (33 w/w % Ni) (Jiménez-González et al., 2015) for methane reforming. It would be therefore of interest to further investigate the viability of this kind of samples for processing more complex fuels by simpler reforming strategies such as partial oxidation.

## 2. Experimental

The spinel-derived Ni/Al<sub>2</sub>O<sub>3</sub> catalyst was synthesised by co-precipitation according to the following procedure. Hence, the process was conducted by the drop-by-drop addition under constant stirring of a 0.6 M solution of NH<sub>4</sub>OH into an aqueous slurry of a mixture of Ni(CH<sub>3</sub>-COO)<sub>2</sub>·4H<sub>2</sub>O and Al(NO<sub>3</sub>)<sub>3</sub>·9H<sub>2</sub>O (1:2 Ni/Al molar ratio) and crushed  $\gamma$ -Al<sub>2</sub>O<sub>3</sub> (133 m<sup>2</sup> g<sup>-1</sup>, 0.3-0.5 mm, SA 6173, Saint-Gobain) to obtain 17 w/w % nickel loading. The temperature was kept at 25 °C during the precipitation and the pH was fixed at 8. Afterwards the precipitate was aged for 30 min before being filtered and washed with hot deionised water. The sample was dried at 110 °C overnight and then calcined at 850 °C in static air for 4 h at a heating rate of 10 °C min<sup>-1</sup>. As a reference reforming catalyst, a commercial powdered Rh-based catalyst was used (1 %Rh/Al<sub>2</sub>O<sub>3</sub>, BET surface area = 132 m<sup>2</sup> g<sup>-1</sup>, Alfa Aesar), which has been calcined at 700 °C in static air for 4 h with the same heating rate. Then pellets were prepared by compressing the powders into flakes in a hydraulic press (Atlas Series Manual Hydraulic Press, Specac), crushing and sieving (0.3-0.5 mm).

### 2.1 Catalyst characterisation

The nickel-based catalyst was characterised by N<sub>2</sub> physisorption at -196 °C, wavelength dispersive X-ray fluorescence (WDXRF), X-ray diffraction (XRD), X-ray photoelectron spectroscopy (XPS), transmission electron microscopy (TEM), temperature programmed reduction with hydrogen (H<sub>2</sub>-TPR) and temperature programmed desorption of NH<sub>3</sub> (NH<sub>3</sub>-TPD). The spent samples were thoroughly characterised by BET measurements, XRD, TEM, thermogravimetry coupled to mass spectrometry (TGA-MS) and Raman spectroscopy. The experimental details of each technique are described elsewhere (Boukha et al., 2014).

### 2.2 Catalytic tests

The catalytic tests for partial oxidation of isooctane were performed using 125 mg of catalyst in a flow reactor operating at atmospheric pressure and at a constant temperature of 600 °C for 30 h. The reaction feed consisted of a mixture of the hydrocarbon (2 vol. % C<sub>8</sub>H<sub>18</sub> and oxygen (molar ratio O/C = 1)) diluted in N<sub>2</sub> with a total flow rate of 800 cm<sup>3</sup> min<sup>-1</sup>. For the partial oxidation runs carried out under humid conditions water was added in order to obtain a H<sub>2</sub>O/C molar ratio of 3. Prior to the reaction, the Ni-based catalyst was activated by reduction with 5 vol. % H<sub>2</sub>/N<sub>2</sub> at 850 °C for 2 h whereas the Rh-based catalyst was reduced using the same reducing stream at 700 °C for 2 h. The liquid hydrocarbon and deionised water feeds have been delivered by two different HPLC pumps and were vaporized separately, then mixed with the other gaseous components (O<sub>2</sub> and/or N<sub>2</sub>) in heated gas lines. Both hot box and feed lines have been heated to a temperature of 180 °C in order to vaporize the liquid feed. The obtained reaction products have been passed through a stainless steel cold water condenser to collect excess water and the unreacted hydrocarbon before injection into the gas chromatograph. Therefore, dry gas stream at the outlet of the reactor was analysed online by a gas chromatograph (MicroGC 3000A, Agilent Technologies) equipped with a TCD detector. Hydrocarbon conversion and yields of H<sub>2</sub>, CO, CO<sub>2</sub> and CH<sub>4</sub> have been determined according to these equations:

$$X, \% = \frac{F_{out}(CO) + F_{out}(CO_2) + F_{out}(CH_4)}{8 \cdot F_{in}(C_8H_{18})} \cdot 100 \quad (1)$$

$$Y(H_2) = \frac{F_{out}(H_2)}{8 \cdot F_{in}(C_8H_{18})} \quad (2)$$

$$Y(CO) = \frac{F_{out}(CO)}{8 \cdot F_{in}(C_8H_{18})} \quad (3)$$

$$Y(CO_2) = \frac{F_{out}(CO_2)}{8 \cdot F_{in}(C_8H_{18})} \quad (4)$$

$$Y(CH_4) = \frac{F_{out}(CH_4)}{8 \cdot F_{in}(C_8H_{18})} \quad (5)$$

where  $F_{in}(C_8H_{18})$  is the inlet molar flow rate of isooctane and  $F_{out}(i)$  is the outlet molar flow rate of the *i*th gaseous component.

The thermodynamic data were calculated via the HSC Chemistry software package by the GIBBS programme using the so-called Gibbs Energy Minimisation Method. In addition to solid carbon, the following gaseous substances were considered: i-C<sub>8</sub>H<sub>18</sub>, CH<sub>4</sub>, O<sub>2</sub>, N<sub>2</sub>, CO, CO<sub>2</sub>, H<sub>2</sub> and H<sub>2</sub>O.

### 3. Results and discussion

#### 3.1 Characterisation of the fresh catalyst

The XRD pattern of the calcined  $\text{NiAl}_2\text{O}_4/\text{Al}_2\text{O}_3$  catalytic precursor is included in Figure 1 ((a) sample). A set of diffractions peaks at  $2\theta = 19.3^\circ$ ,  $31.5^\circ$ ,  $37.2^\circ$ ,  $45.2^\circ$ ,  $59.9^\circ$  and  $65.7^\circ$ , assignable to a nickel aluminate phase, could be identified. In addition to the signals corresponding to  $\text{NiAl}_2\text{O}_4$ , the pattern expectedly should contain the signals attributable to the support. However, since the most intense signals of the alumina are close to those of the spinel phase, the clearest evidence of the presence of the support was perhaps given by the shoulder peak at  $2\theta = 67.0^\circ$ . On the other hand, highly crystalline NiO phase with distinct signals at  $2\theta = 43.5^\circ$  and  $62.9^\circ$  (JCPDS 89-7131) was not found.

The formation of the spinel phase on the surface of the alumina was further corroborated by XPS and UV-vis DRS. As for XPS analysis the Ni  $2p_{3/2}$  spectrum of the calcined samples (Figure 1) was composed of two contributions, namely the main peak corresponding to the  $\text{Ni}^{2+}$  ions and its satellite. The apparent symmetry of this Ni signal suggested the presence of a single homogeneous phase. In fact, the binding energy of this band was centred at about 855.8 eV, which was close to the theoretical value for the nickel aluminate phase (856.0 eV). Moreover, the separation between the principal peak and its satellite (6.1 eV) matched with the reference value (6.3 eV) corresponding to the nickel aluminate spinel (Heracleous et al., 2005).

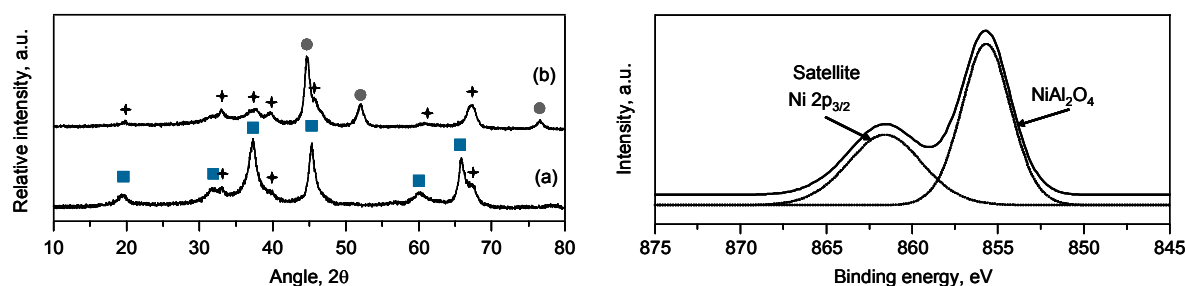


Figure 1: XRD patterns of the calcined (a) and reduced (b) spinel catalyst ( $\text{NiO}$  (●),  $\text{NiAl}_2\text{O}_4$  (■) and  $\text{Al}_2\text{O}_3$  (✦)). XPS spectrum of Ni  $2p_{3/2}$  region of the calcined spinel catalyst.

The structural features of the sample were also examined by UV-Vis DRS (results are not shown here). Thus, in the visible range the bands located at 380 and 720 nm were associated with  $\text{Ni}^{2+}$  ions hosted by octahedral sites. The relative low intensity of these bands implied that the detected  $\text{Ni}^{2+}$  in an octahedral environment was not ascribable to the presence of massively segregated NiO phase but to  $\text{Ni}^{2+}$  ions belonging to the nickel aluminate lattice. The spectrum was also characterised by the presence of an additional intense band at 600–645 nm and shoulders at 550 and 760 nm, thereby evidencing the presence of the tetrahedrally coordinated  $\text{Ni}^{2+}$  ions in the nickel aluminate lattice (Rogers et al., 2016). Additionally, the precursor was analysed by  $\text{H}_2$ -TPR in order to identify the nickel species, their relative abundance and reducibility (Figure 2). It was observed that the  $\text{H}_2$  uptake ( $2.8 \text{ mmol H}_2 \text{ g}^{-1}$ , virtually identical to the theoretical reducibility) was noticeable in a wide temperature range and the reduction process was complete at  $950^\circ\text{C}$ . The main contribution was found at about  $800^\circ\text{C}$  corresponded to the reduction of the  $\text{NiAl}_2\text{O}_4$  spinel. The shoulder identified at  $650^\circ\text{C}$  was assigned to the presence of  $\text{Ni}^{2+}$  ions that were not completely integrated into the spinel while the small consumption detected at  $450^\circ\text{C}$  (lower than 6 %) was related to free NiO species.

The reduced sample (submitted to a reduction step at  $850^\circ\text{C}$  for 2 h with 5 vol. %  $\text{H}_2/\text{N}_2$ ) was analysed by XRD, TEM and  $\text{NH}_3$ -TPD. Recall that this was the activation procedure ( $\text{NiAl}_2\text{O}_4/\text{Al}_2\text{O}_3 \rightarrow \text{Ni}/\text{Al}_2\text{O}_3$ ) used in situ in the reactor prior to reforming runs. The XRD pattern is shown in Figure 1 ((b) sample). It was found that  $\text{Ni}^{2+}$  species were massively reduced into metallic Ni (JCPDS 89-7128, peaks at  $2\theta = 44.6^\circ$ ,  $52.0^\circ$  and  $76.5^\circ$ ). Moreover, the reduction of the spinel phase was complete and simultaneously provoked the formation of the alumina phase. It is worth noting that this phase transformation involved a limited decrease in the surface area from  $94$  to  $84 \text{ m}^2 \text{ g}^{-1}$ . On the other hand, as evidenced by TEM analysis the particle size distribution (around 300 particles were measured) was characterised by a relatively symmetrical band. Most of the particles (99 %) showed a size lower than 20 nm. An average value of 9.5 nm was thus estimated. This value was in good agreement with the mean size calculated by XRD from the Ni(200) signal at  $2\theta = 52^\circ$  (9 nm). On the other hand, the overall acidity ( $\text{NH}_3$ -TPD) of the reduced catalyst was  $302 \mu\text{mol NH}_3 \text{ g}^{-1}$ , significantly lower than that of the bare alumina support ( $630 \mu\text{mol NH}_3 \text{ g}^{-1}$ ). The desorption profile revealed the presence of a band at low temperatures ( $175^\circ\text{C}$ ) accompanied by a second much more intense feature at relatively high temperatures ( $300^\circ\text{C}$ ), the latter being due to a notable fraction of strong acid sites (about 85%) present at the surface of the catalyst.

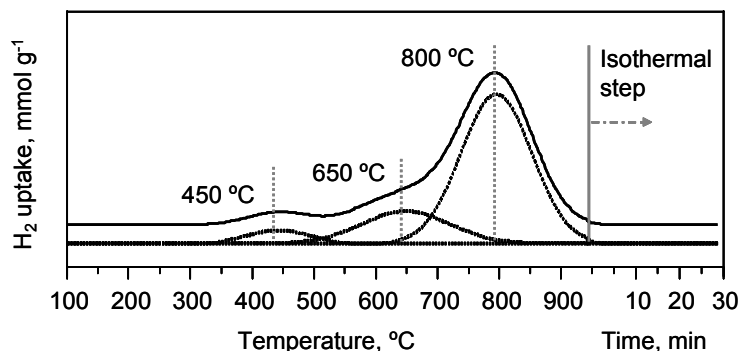


Figure 2:  $H_2$ -TPR profile of the calcined spinel catalyst.

### 3.2 Catalytic behaviour

Figure 3 compares the evolution of isooctane conversion by partial oxidation in absence or presence of water (POX and WET POX, respectively) as a function of time over the Ni and Rh catalysts at 600 °C (7500 mL<sub>C<sub>8</sub>H<sub>18</sub></sub> g<sup>-1</sup> h<sup>-1</sup>; O/C=1). Table 1 shows the values of  $Y(CO)$ ,  $Y(CO_2)$ ,  $Y(CH_4)$ ,  $H_2/CO$  and  $CO/CO_2$  molar ratios for the two investigated catalysts taken the experimental data at the beginning and the end of the runs.

For the POX process, the nickel catalyst showed a relatively low initial conversion (60 %) and a less stable performance with time, while the commercial Rh catalyst was slightly more active (73 %) and exhibited a lower rate of loss of activity. Thus, conversion steadily decreased from 60 to a relatively constant value of 48 % during the first 10h-interval. The loss of activity over the Rh catalyst was also visible but an unchanged conversion (57 %) was attained sooner.

Correspondingly, the yield of hydrogen,  $Y(H_2)$ , decreased from 0.49 to 0.30 for Ni catalyst and from 0.50 to 0.44 for Rh catalyst. While, no significant differences were found in the  $H_2/CO$  molar ratio over the two catalysts, the product distribution for the Ni catalyst was characterised by a lower yield of CO (0.25 compared with 0.35 over the Rh catalyst) and a low  $CO/CO_2$  molar ratio (1.1 compared with 1.8 over the Rh catalyst). This was associated with a higher activity of the noble metal catalyst for the reverse water gas shift reaction that induced a larger presence of CO and/or a favoured transformation of CO into carbon for the nickel catalyst. On the other hand, the  $Y(CH_4)$  was very low (0.01-0.02) for both catalysts.

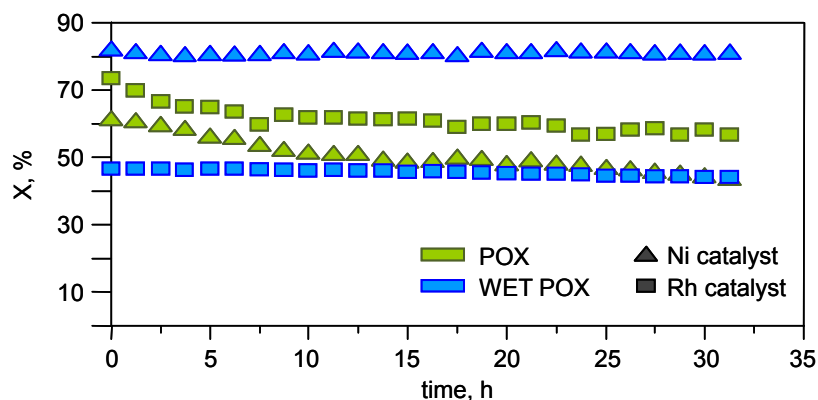


Figure 3: Evolution of isooctane conversion with time in the investigated partial oxidation processes.

The observed deactivation of the Ni catalyst could be related to several causes including coke formation, probably caused by unwanted reactions such as the Boudouard reaction and/or thermal cracking of isooctane, nickel sintering and partial nickel oxidation of the metallic nickel to NiO. Therefore, in order to analyse the extent of these potential deactivating phenomena, the spent Ni catalyst was characterised by TGA-MS, TEM, BET measurements, XRD and Raman spectroscopy. As revealed by TGA-MS a notable formation of coke of about 83 wt % was observed (Figure 4). This finding was related to the substantial strong surface acidity of the catalyst. In accordance with Westrich et al. (2010), the two distinct oxidation peaks at 530 and 570 °C (Figure 4) can be attributed to the combustion of filamentous carbon present on the catalyst. The absence of oxidation peaks below 450 °C seems to indicate that the sample did not contain appreciable amounts of coating carbon. In line with the temperature-programmed oxidation profiles, TEM images confirmed that the spent sample was

mainly covered with filamentous carbon which in turn had an effect on its textural properties as well. Indeed, the specific surface area markedly increased (from 84 to 117 m<sup>2</sup> g<sup>-1</sup>) owing to the contribution of the porosity of the deposited carbon filaments. For the Rh catalyst, it was observed that the considerably lower coke deposition (slightly larger than 2 wt %) did have a clear negative influence on stability. In this case, encapsulating coke was mainly formed given the relatively low combustion temperatures (about 375 °C), the absence of filamentous carbon (as revealed by TEM images of the spent sample) and the observed decrease in specific surface area (from 132 to 114 m<sup>2</sup> g<sup>-1</sup>).

Table 1: Behaviour of the investigated catalysts with time for the partial oxidation of isooctane in the absence or presence of water.

	POX				WET POX	
	Ni/Al <sub>2</sub> O <sub>3</sub>		Rh/Al <sub>2</sub> O <sub>3</sub>		Ni/Al <sub>2</sub> O <sub>3</sub>	Rh/Al <sub>2</sub> O <sub>3</sub>
	t=0	t=30 h	t=0	t=30 h	t=30 h	t=30 h
X, %	60	48	73	57	81	46
Y(H <sub>2</sub> )	0.49	0.30	0.50	0.44	1.30	0.41
Y(CO)	0.36	0.25	0.46	0.35	0.16	0.13
Y(CO <sub>2</sub> )	0.22	0.22	0.41	0.20	0.59	0.32
Y(CH <sub>4</sub> )	0.05	0.01	0.20	0.02	0.06	0.01
H <sub>2</sub> /CO	1.5	1.3	1.4	1.4	8.9	3.6
CO/CO <sub>2</sub>	1.6	1.1	2.0	1.8	0.3	0.4

On the other hand, the diffraction pattern of the post-run nickel catalyst also revealed the presence of large amounts of coke as evidenced by the characteristic peak of graphitic carbon at  $2\theta = 26.3^\circ$  (JCPDS 89-8487). However, since the absence of amorphous carbon could not be ruled out by XRD, the spent catalyst was characterised by Raman spectroscopy as well. Hence, two distinct bands were detected at 1340 cm<sup>-1</sup> (the so-called D band) attributed to the defective and disordered structures and 1580 cm<sup>-1</sup> (the so-called G band) attributed to ordered graphitic coke (Yi et al., 2006). Thus, it was found that both amorphous and graphitic filamentous carbon were present with an I<sub>D</sub>/I<sub>G</sub> intensity ratio of about 1.2. Further, XRD analysis of the used samples also suggested the partial oxidation of the active phase into inactive NiO as evidenced by the signal at  $2\theta = 43.5^\circ$ . Besides, the average Ni particle size estimated by TEM suggested that a slight sintering occurred with an increase in the size from 9 to 11 nm. Although these two findings may also induce a decrease in conversion with time on stream, it is however believed that, judging from the extent of these phenomena, these were of secondary importance in comparison with coke formation.

In spite of the fact that the behaviour of the Ni catalyst in the reforming process pointed out that the synthesis route based on the use of nickel aluminate as precursor was attractive, it was also clear that the reforming of liquid hydrocarbons by partial oxidation would surely require higher reaction temperatures to partially avoid coking and/or the addition of water to notably favour the gasification of deposited coke (Vivanpatarakij et al., 2014). Particularly our attention was focused on this last strategy. Therefore new catalytic runs were carried out ( $C_8H_{18} + 3.5O_2 + H_2O \rightarrow 8CO + 10H_2$ ;  $\Delta H_R(25^\circ C) = -385 \text{ kJ mol}^{-1}$ ) in presence of water ( $H_2O/C = 3$ ) in the feedstream resulting in the so-called WET POX process (which also could be seen as an oxidative steam reforming). The same operation conditions were examined, namely 7500 mL C<sub>8</sub>H<sub>18</sub> g<sup>-1</sup> h<sup>-1</sup>; O/C=1; 600°C, 30 h.

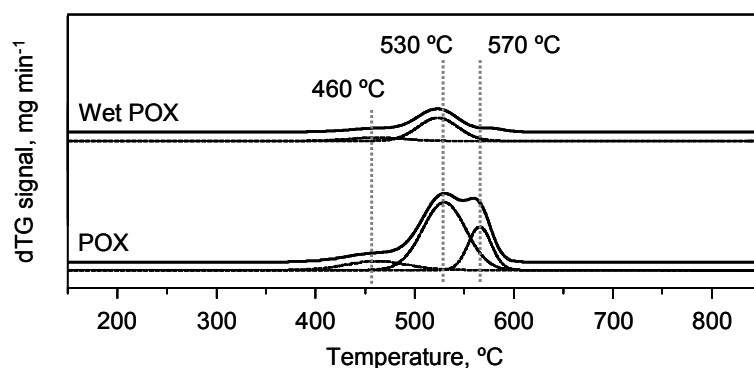


Figure 4: DTG signal of the combustion of deposited coke on the spent Ni catalyst.

Results showed in Figure 1 were very promising since a noticeably higher conversion (81 %) and, perhaps more importantly, a marked stability were noticed for the Ni catalyst. This performance revealed that WET POX reforming of isooctane over the spinel-derived nickel catalyst was a viable strategy. Additional beneficial effects related to the presence of water were also observed in terms of a higher H<sub>2</sub>/CO molar ratio (close to 9) and a lower CO/CO<sub>2</sub> ratio (<0.3) owing to the promotion of the water gas shift reaction.

The post-run spent sample subjected to WET POX was also thoroughly characterised. The most important feature was that the amount of coke was considerably reduced to about 24 % (Figure 4). Although XRD analysis and TEM images evidenced that the morphology was filamentous as well, its chemical nature was less recalcitrant as oxidation at high temperatures (570 °C) was not observed. In view of these results, coke formation in this reforming process apparently did not lead to deactivation, thereby suggesting that the accessibility to active nickel sites was not affected to a large extent.

#### 4. Conclusions

The production of H<sub>2</sub>-rich streams by partial oxidation of isooctane combined with the presence of water was feasible over a 17 %Ni/Al<sub>2</sub>O<sub>3</sub> catalyst derived from nickel aluminate as precursor. The good performance was related to the relatively small size of nickel particles (9 nm). Water was required in order to minimise coke formation owing to thermal cracking of the feed and/or the Boudouard reaction. Filamentous carbon was formed although accessibility to active sites was not negatively impacted since high conversion and remarkable stability were noted. Further, the Ni-based catalyst exhibited a better performance in terms of isooctane conversion and yield of H<sub>2</sub> than that shown by a commercial Rh-based catalyst (1 % Rh/Al<sub>2</sub>O<sub>3</sub>).

#### Acknowledgments

The authors wish to thank the financial support for this work provided by the Ministry of Economy and Competitiveness (ENE2013-41187-R), the Basque Government (PRE\_2013\_2\_453, IT657-13) and the University of The Basque Country (UFI 11/39). Technical and human support from SGIker is also gratefully acknowledged.

#### Reference

- Boukha Z., Jiménez-González C., de Rivas B., González-Velasco J.R., Gutiérrez-Ortiz J.I., López-Fonseca R., 2014, Synthesis, characterisation and performance evaluation of spinel-derived Ni/Al<sub>2</sub>O<sub>3</sub> catalysts for various methane reforming reactions, *Appl. Catal. B: Environ.*, 158-159, 190-201.
- Heracleous E., Leeb A.F., Wilson K., Lemonidou A.A., 2005, Investigation of Ni-based alumina-supported catalysts for the oxidative dehydrogenation of ethane to ethylene: structural characterization and reactivity studies, *J. Catal.*, 231, 159-171.
- Jiménez-González C., Boukha Z., de Rivas B., Delgado J.J., Cauqui M.A., González-Velasco J.R., Gutiérrez-Ortiz J.I., López-Fonseca R., 2013, Structural characterisation of Ni/alumina reforming catalysts activated at high temperatures, *Appl. Catal. A: Gen.*, 466, 9-20.
- Li Y., Zhang B., Xie X., Liu J., Xu Y., Shen W., 2006, Novel Ni catalysts for methane decomposition to hydrogen and carbon nanofibers, *J. Catal.*, 238, 412-424.
- López-Fonseca R., Jiménez-González C., de Rivas B., Gutiérrez-Ortiz J.I., 2012, Partial oxidation of methane to syngas on bulk NiAl<sub>2</sub>O<sub>4</sub> catalyst. Comparison with alumina supported nickel, platinum and rhodium catalysts, *Appl. Catal. A: Gen.*, 437-438, 53-62.
- Moon D.J., Ryu J.W., Lee S.D., Lee B.G., Ahn B.S., 2004, Ni-based catalyst for partial oxidation reforming of isooctane, *Appl. Catal. A: Gen.*, 272, 53-60.
- Rogers J.L., Mangarella M.C., D'Amico A.D., Gallagher J.R., Dutzer M.R., Stavitski E., Miller J.T., Sievers C., 2016, Differences in the nature of active sites for methane dry reforming and methane steam reforming over nickel aluminate catalyst, *ACS Catal.*, 6, 5873-5886.
- Vivanpatarakij S., Rulerk D., Assabumrungrat S., 2014, Removal of tar from biomass gasification process by steam reforming over nickel catalysts, *Chemical Engineering Transactions*, 37, 205-210, DOI: 10.3303/CET1437035
- Westrich T.A., Chen X., Schwank J.W., 2010, Isooctane decomposition and carbon deposition over ceria-zirconia supported nickel catalysts, *Appl. Catal. A: Gen.*, 386, 83-93.